

Probing the QCD Critical End Point with Finite-Size Scaling of Net-Baryon Cumulant Ratios

Roy A. Lacey^{1,*}

¹*Department of Chemistry, Stony Brook University,
Stony Brook, NY, 11794-3400, USA*

(Dated: November 15, 2024)

The search for the Quantum Chromodynamics (QCD) critical end point (CEP) is a central focus in heavy-ion physics, as it provides insights into the phase structure of strongly interacting matter under extreme conditions. Finite-size scaling (FSS) analysis is applied to explore the critical behavior of cumulant ratios C_2/C_1 , C_3/C_2 , C_4/C_2 , C_3/C_1 , and C_4/C_1 , measured in Au+Au collisions across the Beam Energy Scan (BES) range of 7.7 to 200 GeV. The scaling functions for these ratios reveal non-monotonic patterns near the CEP, where critical fluctuations appear in distinct scaling behavior. A consistent scaling pattern emerges at $\sqrt{s}_{\text{CEP}} = 31.0$ GeV, corresponding to $\mu_{B,\text{CEP}} \approx 134.3$ MeV and $T_{\text{CEP}} \approx 155$ MeV, derived from the freeze-out curve. The FSS analysis shows upward divergence of C_2/C_1 and C_4/C_1 , and downward divergence of C_3/C_2 and C_4/C_2 , consistent with theoretical expectations for critical dynamics. These findings validate the robustness of these cumulant ratios as probes for the CEP, offering structured evidence for critical behavior in QCD matter.

PACS numbers: 25.75.-q, 25.75.Dw, 25.75.Ld

The search for the Quantum Chromodynamics (QCD) critical end point (CEP) is a key objective in heavy-ion physics, offering insights into the behavior of strongly interacting matter under extreme conditions. The CEP marks the boundary between a first-order phase transition and a smooth crossover in the QCD phase diagram, analogous to the liquid-gas critical point in water [1, 2].

To probe the CEP, heavy-ion collision experiments, such as the Beam Energy Scan (BES) program at the Relativistic Heavy Ion Collider (RHIC), measure variations in cumulants of the net-baryon number distribution across a range of collision energies and for several centralities at each beam energy [3]. Cumulants are statistical measures that describe the shape of a distribution, capturing moments such as the mean (first-order cumulant, C_1), variance (second-order cumulant, C_2), skewness (third-order cumulant, C_3), and kurtosis (fourth-order cumulant, C_4). While lower-order cumulants, like C_1 and C_2 , reflect basic properties such as the mean and variance, higher-order cumulants, such as C_3 and C_4 , are particularly sensitive to non-Gaussian behavior. Ratios of these cumulants, such as C_2/C_1 , C_3/C_2 , and C_4/C_2 , help monitor potential deviations from monotonic trends, providing valuable insights into critical fluctuations associated with the CEP.

Identifying the CEP in heavy-ion collisions presents notable challenges due to finite-size and finite-time effects that can dampen or distort signatures of criticality. In finite systems, true phase transitions are replaced by smooth crossovers, limiting the development of long-wavelength modes that are crucial for observable critical fluctuations. Additionally, the short-lived nature of the fireball means there is insufficient time for long-wavelength fluctuations to fully develop, which restricts the correlation length and limits the extent of critical fluctuations, complicating experimental detection.

Direct observation of non-monotonic patterns in cumulant ratios, as might be expected in the beam energy dependence of raw data, is challenging due to the combined constraints

of finite size and finite time. Finite-size scaling (FSS) offers a framework to interpret the scaling behavior of these ratios effectively when finite-time effects are not dominant. FSS can help uncover non-monotonic signals when finite-size effects are significant, though finite-time constraints may moderate these characteristics. Conversely, when finite-time effects dominate, the growth of correlation lengths and the emergence of critical signals may be significantly suppressed, impacting their visibility even with FSS. Ratios such as C_2/C_1 and C_3/C_2 , which benefit from volume cancellation, are relatively resilient to finite-time effects because they capture lower-order fluctuations that develop more rapidly than higher-order, non-Gaussian fluctuations. This resilience supports their utility in extracting susceptibility curves and enhancing the search for the CEP by providing robust insights into critical responses [4].

Non-perturbative QCD structures, such as baryon junctions, could play a crucial role in enhancing cumulant ratios like C_2/C_1 , C_3/C_2 , and higher-order ratios such as C_4/C_2 through increased baryon stopping at lower beam energies [5–7]. These structures promote substantial baryon density fluctuations, especially in regions of the QCD phase diagram where baryon stopping is pronounced. Near the CEP, such fluctuations could seed critical dynamics, amplifying compressibility, skewness, and kurtosis as captured by these cumulant ratios [4, 8]. This potential link between non-perturbative QCD phenomena and critical dynamics enhances the sensitivity of cumulant ratios to CEP-related fluctuations, making them an essential consideration in efforts to probe critical behavior.

Finite-size scaling is essential for understanding the scaling behavior of cumulant ratios in heavy-ion collisions, helping to identify genuine critical phenomena and distinguish them from finite-size artifacts. Near the CEP, cumulant ratios follow the FSS relations:

$$\frac{C_2}{C_1} = L^{\gamma/\nu} f_{21}(tL^{1/\nu}, hL^{\Delta/\nu}), \quad \frac{C_3}{C_2} = L^{-\gamma/\nu} f_{32}(tL^{1/\nu}, hL^{\Delta/\nu}),$$

$$\frac{C_4}{C_2} = L^{-\gamma/\nu} f_{42}(tL^{1/\nu}, hL^{\Delta/\nu}), \quad \frac{C_3}{C_1} = L^{-(d-\gamma)/\nu} f_{31}(tL^{1/\nu}, hL^{\Delta/\nu}),$$

$$\frac{C_4}{C_1} = L^{(d+\alpha)/\nu} f_{41}(tL^{1/\nu}, hL^{\Delta/\nu}),$$

where L represents the system size, generally proportional to the fireball volume in heavy-ion collisions, and $t = (T - T_{\text{CEP}})/T_{\text{CEP}}$ is the reduced temperature with T_{CEP} as the critical temperature. The external field $h = (\mu_B - \mu_{B,\text{CEP}})/\mu_{B,\text{CEP}}$ is defined via the baryon chemical potential μ_B and its critical value $\mu_{B,\text{CEP}}$. Here, d is the spatial dimensionality, and γ , ν , α , and Δ are critical exponents that define the scaling behavior. The functions f_{21} , f_{32} , f_{42} , f_{31} , and f_{41} are universal scaling functions associated with each cumulant ratio.

This FSS framework provides a structured approach to studying critical behavior in finite systems, such as the hot, dense fireball produced in heavy-ion collisions near the QCD critical end point (CEP). Applying FSS across multiple cumulant ratios strengthens the reliability of CEP identification by enhancing insights into the critical fluctuations in QCD matter. By comparing density-driven and field-driven scaling paths, FSS confirms the universality of the CEP, as both approaches are expected to converge on the same location for the CEP. Furthermore, FSS enables assessment of the impact of finite-time effects on scaling fidelity, allowing for a more accurate interpretation of scaling signals and reinforcing the robustness of CEP identification.

Distinct cumulant ratios— C_2/C_1 , C_3/C_2 , C_3/C_1 , C_4/C_1 , and C_4/C_2 —provide essential insights into the critical dynamics near the CEP. Ratios such as C_2/C_1 and C_3/C_2 , which benefit from volume cancellation, are particularly robust for FSS analyses and serve as intensive quantities effective in detecting criticality signals. The upward divergence of C_2/C_1 , related to increasing susceptibility, reflects system compressibility as it approaches the CEP. Conversely, C_3/C_2 , associated with skewness, diverges downward, capturing asymmetry in the fluctuation distribution and highlighting non-Gaussian features.

The ratio C_4/C_2 , also benefiting from volume cancellation, is sensitive to higher-order non-Gaussian fluctuations and is expected to diverge downward near the CEP, though it may be more susceptible to finite-time effects due to the time required for such fluctuations to develop fully.

Higher-order ratios, C_3/C_1 and C_4/C_1 , provide further perspectives on critical behavior. Although only partially volume-cancelled, C_4/C_1 displays an upward divergence related to kurtosis and non-Gaussian fluctuations, while C_3/C_1 diverges downward, reflecting suppression of skewness relative to the mean. The partial volume cancellation in these ratios may affect their sensitivity to critical dynamics, yet they still contribute valuable information.

By analyzing these cumulant ratios together, scaling studies gain reliability and enhance CEP identification by ensuring each ratio's unique scaling behavior is used to build a comprehensive picture of the critical response near the CEP.

Effective application of the FSS relations requires robust knowledge of the thermodynamic scaling variables—the reduced temperature t and external field h —that define the trajectory toward the CEP. However, directly accessing t and h is challenging in heavy-ion collisions. To address this, beam energy (\sqrt{s}) serves as a practical proxy for both μ_B and T , enabling exploration of thermodynamic conditions through scaling variables based on \sqrt{s} . By utilizing the freeze-out curve to parametrize the path to the CEP, \sqrt{s} can reflect both density-driven and field-driven trajectories, with field-driven dynamics especially relevant for observables sensitive to μ_B , such as net-baryon fluctuations.

- **Field-Driven Scaling Variable $h_{\sqrt{s}}$:** Net-baryon fluctuations, which are primarily field-driven and sensitive to μ_B variations [9, 10], can be analyzed using $h_{\sqrt{s}}$:

$$h_{\sqrt{s}} = \frac{(1/\mu_B) - (1/\mu_{B,\text{CEP}})}{(1/\mu_{B,\text{CEP}})} \approx \frac{\sqrt{s} - \sqrt{s}_{\text{CEP}}}{\sqrt{s}_{\text{CEP}}},$$

where $1/\mu_B \propto \sqrt{s}$ [11, 12], and \sqrt{s}_{CEP} corresponds to the critical $\mu_{B,\text{CEP}}$. Using finite-size scaling with $h_{\sqrt{s}}$, \sqrt{s}_{CEP} can be extracted and subsequently mapped to both T_{CEP} and $\mu_{B,\text{CEP}}$ via the freeze-out curve [11, 12], effectively capturing field-driven dynamics.

- **Density-Driven Scaling Variable $t_{\sqrt{s}}$:** With the critical values \sqrt{s}_{CEP} and $\mu_{B,\text{CEP}}$ identified via $h_{\sqrt{s}}$, the density-driven scaling variable $t_{\sqrt{s}}$ is defined as:

$$t_{\sqrt{s}} = \frac{\sqrt{s} - \sqrt{s}_{\text{CEP}}}{\sqrt{s}_{\text{CEP}}}.$$

This approach enables $t_{\sqrt{s}}$ to act as a density-driven proxy, tracking deviations from critical behavior. Interpreting μ_B -dependent fluctuations with respect to the critical $\mu_{B,\text{CEP}}$ derived from the field-driven analysis ensures consistency across scaling variables.

This dual approach—starting with $h_{\sqrt{s}}$ to determine \sqrt{s}_{CEP} and confirming consistency with $t_{\sqrt{s}}$ —allows for a robust estimate of the CEP. By aligning density and field trajectories, this analysis leverages \sqrt{s} as a unified experimental proxy, yielding a reliable location for the CEP in both temperature and chemical potential space.

The size parameter $\bar{R} = L$ used in finite-size scaling (FSS) analysis is derived from Monte Carlo Glauber (MC-Glauber) calculations [13, 14] for various collision centralities at each beam energy, detailing the nuclear geometry involved in each collision. In the MC-Glauber model, nucleons participating in an initial inelastic nucleon-nucleon (N+N) interaction form the participant set (N_{part}).

The transverse distribution of these participants in the X-Y plane is quantified by the root-mean-square (RMS) widths σ_x and σ_y , calculated along the principal axes of the participant zone. The transverse system size, \bar{R} , is then defined as $\frac{1}{\bar{R}} =$

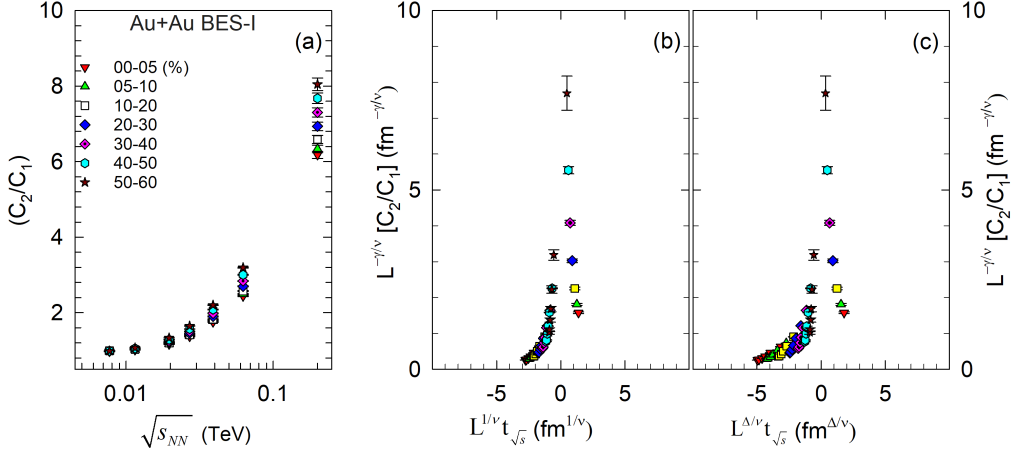


FIG. 1. (Color Online) Panel (a) presents the beam energy dependence of $C_2(\text{cent})/C_1(\text{cent})$ for Au+Au collisions across multiple centralities, as indicated. Panels (b) and (c) display the resulting density-driven and field-driven scaling functions obtained through finite-size scaling of the data in panel (a). The scaling functions exhibit the anticipated upward divergence in the vicinity of the CEP.

$\sqrt{\left(\frac{1}{\sigma_x^2} + \frac{1}{\sigma_y^2}\right)}$ [15], ensuring a meaningful representation of the system's geometric spread.

For FSS, the **relative magnitudes** of L across different energies and centralities are crucial, allowing for robust scaling analyses that account for possible model uncertainties in the absolute size of L . This approach facilitates the comparison of systems of varying sizes while maintaining the integrity of universal scaling behavior.

The parameter \bar{R} encapsulates the spatial extent of the colliding system. The three HBT radii— R_{out} , R_{side} , and R_{long} —characterize the space-time dimensions of the emitting sources and show a linear dependence on \bar{R} across the studied beam energy range [16, 17]. This consistency supports \bar{R} as a reliable measure of transverse size in FSS studies.

Systematic uncertainties for \bar{R} from varying model parameters within the MC-Glauber framework are estimated at less than 2% [14], confirming the robustness of \bar{R} for scaling analyses across centralities and beam energies. Consequently, \bar{R} serves as a practical metric for probing universal scaling in heavy-ion collisions.

To apply finite-size scaling relations to experimental data, the cumulant ratios C_2/C_1 , C_3/C_2 , C_4/C_2 , C_3/C_1 , and C_4/C_1 , measured in Au+Au collisions across the full Beam Energy Scan (BES) range from 7.7 to 200 GeV, are utilized [18]. The data spans several collision centralities, providing a comprehensive view of scaling behavior across varying system sizes. These ratios, sensitive to critical fluctuations, serve as effective probes for examining the QCD critical end point (CEP) through their scaling properties.

This analysis employs the scaling variables $t_{\sqrt{s}}$ and $h_{\sqrt{s}}$ to explore critical behavior across the BES-I energy range via FSS. Figs. 1 and 2 illustrate the scaling procedure for C_2/C_1 and C_3/C_2 , respectively. Figs. 1 (a) and 2 (a) show that finite-size effects mask the non-monotonic patterns that would in-

dicate the CEP. By contrast, Figs. 1(b) and (c) and Figs. 2(b) and (c) reveal clear indications of non-monotonic patterns in the scaling functions, reflecting the upward divergence of C_2/C_1 (linked to increasing compressibility and susceptibility) and the downward divergence of C_3/C_2 (indicating skewness and asymmetry in fluctuations). The scaling fidelity for C_2/C_1 is high for both density- and field-driven scaling, suggesting limited influence from finite-time effects for this ratio. The fidelity for C_3/C_2 is also good but somewhat lower than for C_2/C_1 , possibly indicating the expected greater influence of finite-time effects on C_3/C_2 . Notably, the scaling behavior for proxy compressibility data reported in [4] shows similarly robust scaling functions, yielding values of $\mu_{B,\text{CEP}}$ and T_{CEP} consistent with those derived in the present analysis.

Figure 3 shows the field-driven scaling functions for C_4/C_2 , C_3/C_1 , and C_4/C_1 . Panel (a) shows the expected downward divergence near the CEP for C_4/C_2 , tied to higher-order, non-Gaussian fluctuations. This divergence may be of smaller magnitude, possibly due to finite-time effects. Panel (b) also shows the anticipated downward divergence near the CEP for C_3/C_1 , reflecting skewness suppression, but with reduced scaling fidelity, likely due to partial volume cancellation. In contrast, panel (c) shows the expected upward divergence near the CEP for C_4/C_1 , highlighting the contribution of kurtosis and non-Gaussian fluctuations, with relatively good scaling fidelity.

The scaling functions presented in Figs. 1 - 3 were all obtained using $\sqrt{s}_{\text{CEP}} = 31.0 \text{ GeV}$. The corresponding values $\mu_{B,\text{CEP}} \approx 134.3 \text{ MeV}$ and $T_{\text{CEP}} \approx 155 \text{ MeV}$, obtained from the freeze-out curve [11, 12], provide a unified reference for critical fluctuations. This combined approach leverages the unique scaling characteristics of each cumulant ratio and carefully accounts for finite-time and volume effects, enhancing the reliability of scaling analyses and supporting CEP identification.

In summary, the finite-size scaling (FSS) analysis of cumu-

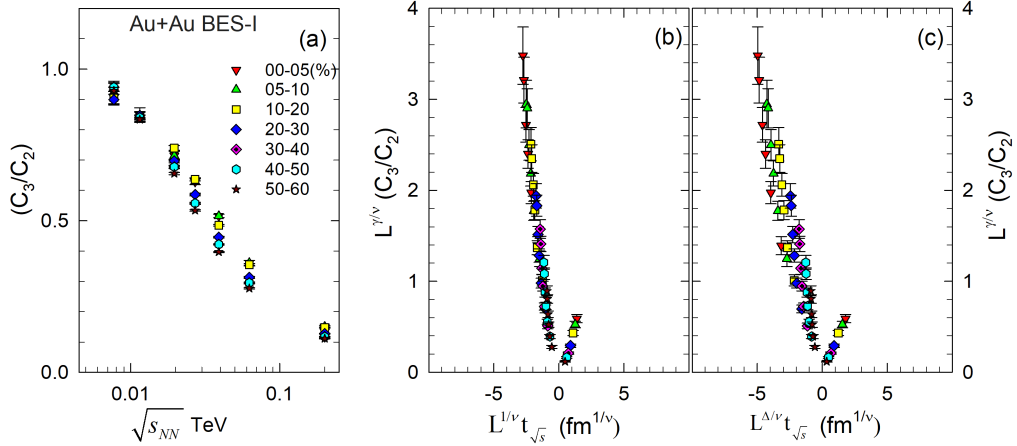


FIG. 2. (Color Online) Panel (a) presents the beam energy dependence of $C_3(\text{cent})/C_2(\text{cent})$ for Au+Au collisions across multiple centralities, as indicated. Panels (b) and (c) display the resulting density-driven and field-driven scaling functions obtained through finite-size scaling of the data in panel (a). The scaling functions exhibit the anticipated downward asymmetric divergence in the vicinity of the CEP.

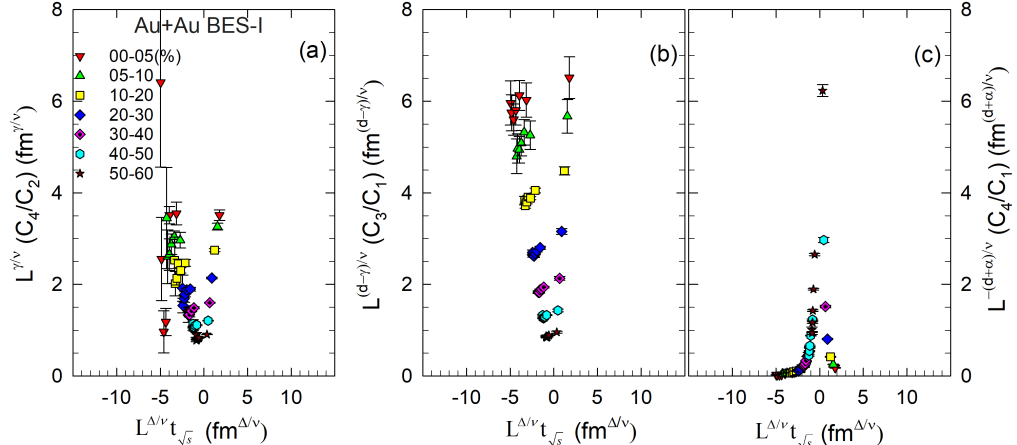


FIG. 3. (Color Online) Panels (a), (b), and (c) display the field-driven scaling functions obtained through finite-size scaling of the data for $C_4(\text{cent})/C_2(\text{cent})$, $C_3(\text{cent})/C_1(\text{cent})$, and $C_4(\text{cent})/C_1(\text{cent})$, respectively. The scaling functions exhibit the anticipated divergences in the vicinity of the CEP.

lant ratios C_2/C_1 , C_3/C_2 , C_4/C_2 , C_3/C_1 , and C_4/C_1 measured in Au+Au collisions across the BES energy range provides a compelling framework for locating the QCD critical end point (CEP). The scaling behavior observed for these ratios, particularly the upward divergence of C_2/C_1 and C_4/C_1 and the downward divergence of C_3/C_2 and C_4/C_2 , aligns with theoretical expectations for critical dynamics near the CEP. The analysis, anchored at $\sqrt{s}_{\text{CEP}} = 31.0$ GeV and corresponding to $\mu_{B,\text{CEP}} \approx 134.3$ MeV and $T_{\text{CEP}} \approx 155$ MeV, offers a consistent reference across both field-driven and density-driven scaling variables. Moreover, the scaling fidelity observed, despite finite-time effects, underscores the robustness of these cumulant ratios as probes of critical behavior. Together, these findings enhance the reliability of CEP identifi-

cation and contribute valuable insights into the critical fluctuations in strongly interacting matter, supporting further exploration in the quest to understand the QCD phase structure.

* E-mail: Roy.Lacey@Stonybrook.edu

- [1] M. A. Stephanov, *Prog. Theor. Phys. Suppl.* **153**, 139 (2004), [arXiv:hep-ph/0402115](https://arxiv.org/abs/hep-ph/0402115).
- [2] K. Rajagopal and F. Wilczek, “The Condensed matter physics of QCD,” in *At the frontier of particle physics. Handbook of QCD. Vol. 1-3*, edited by M. Shifman and B. Ioffe (2000) pp. 2061–2151, [arXiv:hep-ph/0011333](https://arxiv.org/abs/hep-ph/0011333).
- [3] J. Adam *et al.* (STAR), *Phys. Rev. Lett.* **126**, 092301 (2021), [arXiv:2001.02852 \[nucl-ex\]](https://arxiv.org/abs/2001.02852).

- [4] R. A. Lacey, *Phys. Rev. Lett.* **114**, 142301 (2015), arXiv:1411.7931 [nucl-ex].
- [5] D. Kharzeev, *Phys. Lett. B* **378**, 238 (1996), arXiv:nucl-th/9602027.
- [6] D. Kharzeev and M. Nardi, *Phys. Lett. B* **507**, 121 (2001), arXiv:nucl-th/0012025.
- [7] R. A. Lacey, (2024), arXiv:2410.22688 [nucl-ex].
- [8] M. A. Stephanov, *Phys. Rev. Lett.* **102**, 032301 (2009), arXiv:0809.3450 [hep-ph].
- [9] M. Asakawa, U. W. Heinz, and B. Muller, *Phys. Rev. Lett.* **85**, 2072 (2000), arXiv:hep-ph/0003169.
- [10] M. A. Stephanov, *J. Phys. G* **38**, 124147 (2011).
- [11] J. Cleymans, H. Oeschler, K. Redlich, and S. Wheaton, *Phys. Rev. C* **73**, 034905 (2006), arXiv:hep-ph/0511094.
- [12] A. Andronic *et al.*, *Nucl. Phys. A* **837**, 65 (2010), arXiv:0911.4806 [hep-ph].
- [13] M. L. Miller, K. Reygers, S. J. Sanders, and P. Steinberg, *Ann. Rev. Nucl. Part. Sci.* **57**, 205 (2007), arXiv:nucl-ex/0701025.
- [14] R. A. Lacey, R. Wei, N. N. Ajitanand, and A. Taranenko, *Phys. Rev. C* **83**, 044902 (2011), arXiv:1009.5230 [nucl-ex].
- [15] R. S. Bhalerao, J.-P. Blaizot, N. Borghini, and J.-Y. Ollitrault, *Phys. Lett. B* **627**, 49 (2005), arXiv:nucl-th/0508009.
- [16] R. A. Lacey, *Nucl. Phys. A* **931**, 904 (2014), arXiv:1408.1343 [nucl-ex].
- [17] A. Adare *et al.* (PHENIX), (2014), arXiv:1410.2559 [nucl-ex].
- [18] M. Abdallah *et al.* (STAR), *Phys. Rev. C* **104**, 024902 (2021), arXiv:2101.12413 [nucl-ex].